

Axisymmetric equilibria with central current reversal caused by non-parallel plasma flow

A. Kuiroukidis¹ and G. N. Throumoulopoulos²

¹ Technological Education Institute of Central Macedonia,
GR 621 24 Serres, Greece

² University of Ioannina, Department of Physics,
Section of Astrophysics, GR 451 10 Ioannina, Greece
Emails: kourouki@astro.auth.gr, gthroum@uoi.gr

Abstract

We obtain analytic solutions of a generalised Grad-Shafranov equation describing steady states with incompressible plasma flow of arbitrary direction, toroidal current reversal and either nested or non-nested magnetic surfaces. It turns out that the component of the flow velocity non parallel to the magnetic field can result in normal equilibria with central current-reversal, i.e. equilibria with nested magnetic surfaces and monotonically varying pressure profiles.

1 Introduction

Advanced confinement in tokamaks is related to Internal Transport Barriers (ITBs) of energy and particle transport (e.g. see the review paper [1]). Experimental evidence indicates that reversed magnetic shear and sheared flow play a role in the establishment of ITBs; specifically according to experimental results of JET [2] and DIII-D [3], on the one hand the reversed magnetic helps in triggering the ITBs development while on the other hand the sheared rotation has an impact on the subsequent growth and allows the formation of strong ITBs. In certain tokamak equilibria with ITBs known as current holes, the central current is nearly zero (e.g. see the review paper [4]). According to current hole experiments in JET [5] and JT-60U [6] the core current density is clamped at zero, indicating the existence of a physical mechanism which prevents it from becoming negative. These observations motivated a number of theoretical studies on the existence of equilibria with current reversal [7]-[23]. The conclusion is that central current reversal in normal equilibria, i.e. global equilibria with nested magnetic surfaces and monotonically varying pressure, can not exist [7]-[10]. Potential physical mechanisms for that

prevention are the influence of a resistive kink magnetohydrodynamic instability [7] and reconnection [10]. However, current-reversal equilibria with non nested magnetic surfaces, i.e. having magnetic lobes, can exist [11]-[25] in consistence with experimental evidence in tokamaks [26]-[29].

The present study was partly motivated by the paper of Ref. [30], according to which toroidal rotation opens up the possibility of normal equilibria with current reversal in the vicinity of the magnetic axis. The purpose of our study is twofold: first to construct axisymmetric equilibria with current reversal and incompressible flow with either nested or non-nested magnetic surfaces, and second to examine the existence of normal stationary equilibria with current reversal near the magnetic axis. The construction is based on a generalized Grad-Shafranov (GGS) equation with incompressible flow (Eq. (1) below) involving five free surface-quantity terms. Specifically a linearised form of that equation is solved analytically.

The GGS equation is briefly reviewed in section 2. Solutions with current density reversal are derived for a toroidal plasma of arbitrary aspect ratio and rectangular poloidal cross section with ITER-like shaping in section 3. Part of the construction regarding two independent solutions of the respective homogeneous partial differential equation is given in Appendix. Section 4 summarizes the conclusions.

2 Generalized Grad-Shafranov equation

We consider the generalized Grad-Shafranov (GGS) equation with incompressible flow [31]-[33]:

$$\begin{aligned} (1 - M_p^2)\Delta^*\psi - \frac{1}{2}(M_p^2)'|\nabla\psi|^2 + \frac{1}{2}\left(\frac{X^2}{1 - M_p^2}\right)' \\ + \mu_0 R^2 P_s' + \mu_0 \frac{R^4}{2} \left[\frac{\varrho(\Phi')^2}{1 - M_p^2} \right]' = 0 \end{aligned} \quad (1)$$

Here, the poloidal magnetic flux function $\psi(R, z)$ labels the magnetic surfaces, where (R, ϕ, z) are cylindrical coordinates with z corresponding to the axis of symmetry; $M_p(\psi)$ is the Mach function of the poloidal fluid velocity with respect to the poloidal Alfvén velocity; $X(\psi)$ relates to the toroidal magnetic field, $B_\phi = I/R$, through $I = X/(1 - M^2)$; $\Phi(\psi)$ is the electrostatic potential; for vanishing flow the surface function $P_s(\psi)$ coincides with the

pressure; B is the magnetic field modulus which can be expressed in terms of surface functions and R ; $\Delta^* = R^2 \nabla \cdot (\nabla / R^2)$; and the prime denotes derivatives with respect to ψ . Because of incompressibility the density $\varrho(\psi)$ is also a surface quantity and the Bernoulli equation for the pressure decouples from (1):

$$P = P_s(\psi) - \varrho \left[\frac{v^2}{2} - \frac{R^2(\Phi')^2}{1 - M_p^2} \right] \quad (2)$$

where v is the velocity modulus. Also, \mathbf{v} can be decomposed in a component parallel and another non-parallel to \mathbf{B} as

$$\mathbf{v} = \frac{M_p}{\sqrt{\varrho}} \mathbf{B} - R \Phi' \mathbf{e}_\phi \quad (3)$$

The quantities $M_p(\psi)$, $X(\psi)$, $P_s(\psi)$, $\varrho(\psi)$ and $\Phi(\psi)$ are free functions. Derivation of (1) and (2) is provided in [31]-[33].

Eq. (1) can be simplified by the transformation

$$u(\psi) = \int_0^\psi [1 - M_p^2(f)]^{1/2} df \quad (4)$$

under which (1) becomes

$$\Delta^* u + \frac{1}{2} \frac{dI^2}{d\psi} + \mu_0 R^2 \frac{dP_s}{du} + \frac{\mu_0}{2} R^4 \frac{dG}{du} = 0 \quad (5)$$

where $G(u) := \varrho(\psi)(d\Phi(u)/du)^2$. Note that no quadratic term as $|\nabla u|^2$ appears any more in (5). Once a solution of (5) is obtained, the equilibrium can be completely constructed with calculations in the u -space.

Instead of (5) we will employ the GGS in the following normalized form

$$\begin{aligned} [\partial_{\rho\rho} - (1/\rho)\partial_\rho + \partial_{\zeta\zeta}]\tilde{u} &+ \frac{1}{2} \frac{d}{d\tilde{u}} \left[\frac{\tilde{X}^2}{1 - \tilde{M}_p^2} \right] + \rho^2 \frac{d\tilde{P}_s}{d\tilde{u}} + \\ &+ \frac{1}{2} \rho^4 \frac{d\tilde{G}}{d\tilde{u}} = 0 \end{aligned} \quad (6)$$

Here, $\rho := R/R_0$, $\zeta := z/R_0$, $\tilde{u} := u/u_0$ (where R_0 is the major radius of the toroidal configuration), $\tilde{P}_s := P_s/P_0$, $\tilde{X} := X/X_0$, $\tilde{G} := G/G_0$, with ITER-relevant data $P_0 = 1.6 \times 10^5 Pa \simeq 1.58 Atm$, $R_0 = 6.2m$, $a = 1.1m$ (where a is the major radius), $u_0^2 := P_0 \mu_0 R_0^4$, $u_0 \simeq 17.23 Wb$, $X_0 := u_0/R_0 = 2.78 Wb/m$,

$I_0 := u_0/\mu_0 R_0 \simeq 2.21 MA$, $G_0 = 4.16 \times 10^3 Kg/m^3 sec^2$. Using the above parametric values the pressure and toroidal current density are given by

$$\begin{aligned}
P(kPa) = & 160\tilde{P}_s(\tilde{u}) - 80 \left[\frac{\tilde{X}^2}{1 - M_p^2} \right] \frac{M_p^2}{\rho^2(1 - M_p^2)} - \\
& - 80 \frac{\rho^2}{(1 - M_p^2)} \tilde{G}(\tilde{u}) + \\
& + 160 \frac{1}{(1 - M_p^2)^{1/2}} \left[\frac{\tilde{X}^2}{1 - M_p^2} \right]^{1/2} \left[\frac{M_p^2}{1 - M_p^2} \right]^{1/2} [\tilde{G}(\tilde{u})]^{1/2} - \\
& - 80 \frac{M_p^2}{1 - M_p^2} [\tilde{u}_\rho^2 + \tilde{u}_\zeta^2] + 160\rho^2 \tilde{G}(\tilde{u})
\end{aligned} \tag{7}$$

$$\begin{aligned}
J_{tor}(MA/m^2) = & 0.057 \frac{1}{\sqrt{1 - M_p^2}} \frac{\tilde{\Delta}^* \tilde{u}}{\rho} + \\
& + 0.0285 \frac{(M_p^2)'}{(1 - M_p^2)^{3/2}} \frac{\tilde{u}_\rho^2 + \tilde{u}_\zeta^2}{\rho}
\end{aligned} \tag{8}$$

We hereafter drop tildes for simplicity and choose the following forms for the poloidal current density, pressure and non-parallel-flow function G :

$$\frac{1}{2} \frac{d}{du} \left[\frac{X^2}{1 - M_p^2} \right] = \alpha_1 + \alpha^2 u \tag{9}$$

$$\frac{dP_s}{du} = -\beta_1 + \alpha^4 u \tag{10}$$

$$\frac{dG}{du} = -\gamma_1 \tag{11}$$

Eqs. (9)-(11) are integrated with zero integration constants for the last two equations and with integration constant α_0 for the first one. Also, following [15] we introduce the new dependent variable $A = u/\rho$ and adopt the boundary condition $u|_b = A|_b = 0$. Additionally, in connection with potential flow-caused central reversal of the toroidal current density the poloidal Mach function is assigned by

$$M_p^2 = M_0^2 u^n \tag{12}$$

where M_0^2 and n relate to the maximum value of the poloidal Mach function on the magnetic axis and the shape of M_p^2 , respectively. This function becomes maximum on axis and vanishes on the boundary; therefore it is peaked on-axis in association with a respective on-axis momentum source. Alternatively, we have employed the off-axis peaked poloidal Mach function

$$M_p^2 = M_0^2 u^m (u_a - u)^n \quad (13)$$

where u_a is the poloidal flux function on the magnetic axis and M_0^2 relates to the maximum of M_p^2 ; the parameters m, n determine the shape of M_p^2 and the position of its maximum, i.e. this maximum corresponds to $mu_a/(m+n)$ with a measure of the profile width being $u_a/(m+n)$.

Furthermore, following [15], [34], we consider a boundary of rectangular cross section so that $\rho \in [1 - \epsilon, 1 + \epsilon]$ and $\zeta \in [-\kappa\epsilon, \kappa\epsilon]$ where $\epsilon := a/R_0 \simeq 0.177$ is the inverse aspect ratio and $\kappa \simeq 1.86$ is the elongation. Thus the boundary value problem for the GGS equation assumes the form

$$\begin{aligned} \left[\frac{1}{\rho} \partial_\rho (\rho \partial_\rho) + \partial_{\zeta\zeta} \right] A + \left(\alpha^2 - \frac{1}{\rho^2} \right) A + \alpha^4 \rho^2 A = \\ = -\frac{\alpha_1}{\rho} + \beta_1 \rho + \frac{1}{4} \gamma_1 \rho^3 \end{aligned} \quad (14)$$

$$A|_b = 0 \quad (15)$$

3 Solutions and equilibrium properties

We consider first the homogeneous boundary value problem and boundary conditions corresponding to Eqs. (14) and (15):

$$\begin{aligned} \left[\frac{1}{\rho} \partial_\rho (\rho \partial_\rho) + \partial_{\zeta\zeta} \right] A + \left(\lambda^2 - \frac{1}{\rho^2} \right) A + \lambda^4 \rho^2 A = 0 \\ A(1 - \epsilon, \zeta) = A(1 + \epsilon, \zeta) = 0 \\ A(\rho, -\kappa\epsilon) = A(\rho, \kappa\epsilon) = 0 \end{aligned} \quad (16)$$

and set $A(\rho, \zeta) = U(\rho)Z(\zeta)$. We thus have

$$\begin{aligned} \frac{d^2 Z}{d\zeta^2} + \nu^2 Z = 0 \\ Z(-\kappa\epsilon) = Z(\kappa\epsilon) = 0 \end{aligned} \quad (17)$$

with solution

$$Z(\zeta) = \cos(\nu_l \zeta), \quad \nu_l = (l + 1/2)\pi/\kappa\epsilon, \quad (l = 0, 1, 2, \dots) \quad (18)$$

Furthermore setting $\lambda_{nl}^2 := \nu_l^2 + \mu_n^2$, ($n = 1, 2, \dots$) we obtain for $U(\rho)$

$$\rho^2 \frac{d^2 U}{d\rho^2} + \rho \frac{dU}{d\rho} + (\mu_n^2 \rho^2 + \lambda_{nl}^4 \rho^4 - 1)U = 0 \quad (19)$$

$$U(1 - \epsilon) = U(1 + \epsilon) = 0 \quad (20)$$

The differential equation (19) is solved in the Appendix and its two independent solutions are hereafter called $J_1(\rho; \mu_n, \nu_l)$ and $Y_1(\rho; \mu_n, \nu_l)$. The eigenfunctions of Eq. (19) are therefore of the form

$$U_{n,l}(\rho) = c_{n,l} J_1(\rho; \mu_n, \nu_l) + Y_1(\rho; \mu_n, \nu_l) \quad (21)$$

and implementing the boundary conditions (20) results in the eigenvalue equations

$$c_{n,l} = -\frac{Y_1((1 - \epsilon); \mu_n, \nu_l)}{J_1((1 - \epsilon); \mu_n, \nu_l)} - J_1((1 + \epsilon); \mu_n, \nu_l) \frac{Y_1((1 - \epsilon); \mu_n, \nu_l)}{J_1((1 - \epsilon); \mu_n, \nu_l)} + Y_1((1 + \epsilon); \mu_n, \nu_l) = 0 \quad (22)$$

The last of Eqs. (22) is solved numerically for μ_1, \dots, μ_{10} since for computational purposes we have retained terms of up to $n = 10$. The dependence of the parameters μ_n as a function of $n = 1, \dots, 10$ (approximated to vary continuously) for $l = 0, 1, 2$ is shown in Fig. 1.

To construct a particular solution of the inhomogeneous Eq. (14) we employ the method of expansion with respect to eigenfunctions [14, 15]; accordingly A is of the form

$$A(\rho, \zeta) = \sum_{n=1}^{N_n} \sum_{l=0}^{N_l} A_{nl} U_{n,l}(\rho) \cos(\nu_l \zeta) \quad (23)$$

with the coefficients A_{nl} to be determined. Here the sums can have an arbitrary number of terms ($N_n = \infty$, and $N_l = \infty$), but for computational purposes we have retained terms of up to $N_n = 10$, $N_l = 4$. Note that the

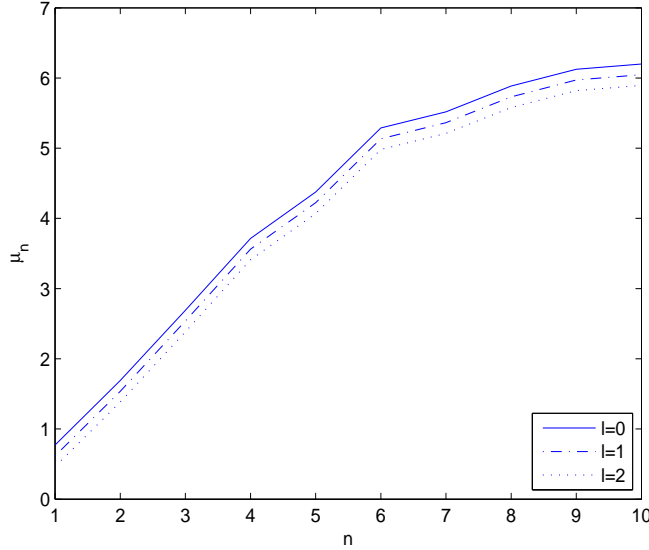


Figure 1: The numerically determined parameters μ_n , from Eq. (22).

functions $U_{n,l}(\rho)$ are *not* orthogonal in the interval $\rho \in [1 - \epsilon, 1 + \epsilon]$. Also (23) satisfies the boundary condition automatically. Then Eq. (14) yields

$$-\frac{\alpha_1}{\rho} + \beta_1 \rho + \frac{1}{4} \gamma_1 \rho^3 = \sum_{n=1}^{10} \sum_{l=0}^4 A_{nl} [(\alpha^2 - \lambda_{n,l}^2) + (\alpha^4 - \lambda_{n,l}^4) \rho^2] U_{n,l}(\rho) \cos(\nu_l \zeta) \quad (24)$$

Thus, due to the non-orthogonality of the functions $U_{n,l}(\rho)$, we multiply Eq. (24) by $U_{n',l'}(\rho) \cos(\nu_{l'} \zeta)$ and integrate in the relevant intervals. We obtain a linear $-(50 \times 50)$ system for the expansion coefficients $A_{n,l}$ which is solved numerically.

Assigning proper values to the free parameters involved in ansatz (9)-(11), as given in Table 1, we have constructed equilibria with reversed current density. Three examples of them are shown in Figs. 2-4. The first equilibrium (Fig. 2) has nested magnetic surfaces and the others (Figs. 3, 4) non-nested ones; specifically the second equilibrium consists of a couple of magnetic lobes with magnetic axes orientated perpendicular to the axis of symmetry (Fig. 3) and the third one has three lobes with magnetic axes orientated parallel to the axis of symmetry (Fig. 4). In the second and third equilibria

Parameters	α_1	β_1	γ_1	α
Fig. 2	5.3	1.3	1.3	5.0
Fig. 3	1.5	1.5	0	3.5
Fig. 4	7.5	7.0	0	6.75

Table 1: Values of the parameters in ansatz (9-11) for the equilibria of Figs. 2-4.

the plasma flows parallel to the magnetic field ($\gamma_1 = 0$). The single magnetic axis of the first equilibrium is located at $\rho \approx 1.002$ and its position remains nearly unaffected when the values of the flow parameters M_0^2 and γ_1 change.

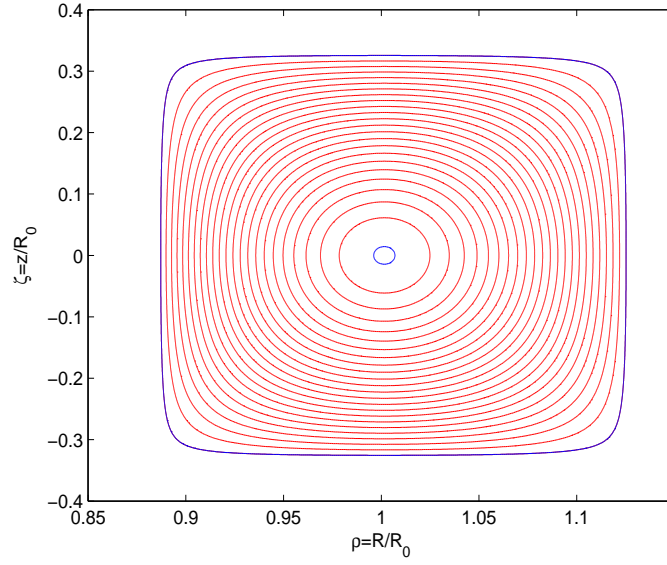


Figure 2: The first equilibrium with nested magnetic surfaces described in the text. The boundary, shown in blue, corresponds to the flux value of $u_b = 0$, while on the magnetic axis we have $u_a = -0.9375$.

We have examined the impact of the flow on the toroidal current density of equilibria with nested magnetic surfaces and found that the non parallel component of the flow can result in current reversal in the region of the magnetic axis. This is illustrated in Fig. 5 corresponding to the peaked

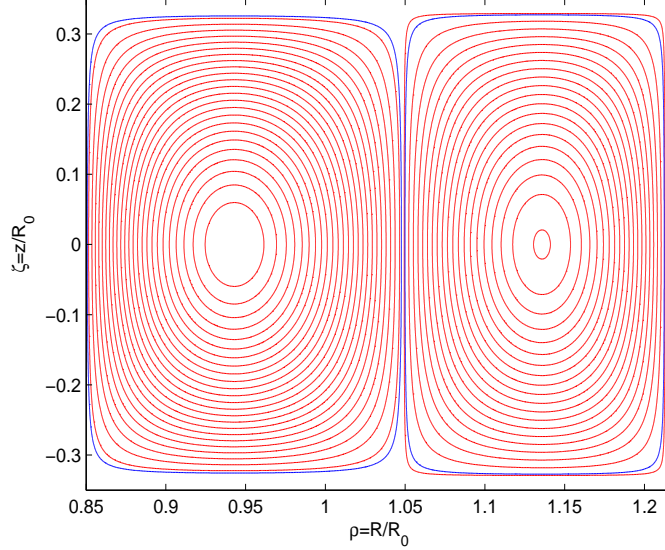


Figure 3: The second equilibrium with non-nested magnetic surfaces described in the text. The boundary of the magnetic lobes, shown in blue, corresponds to the flux value of $u_b = 0$, while on the left magnetic axis we have $u_{left} = -0.94$ and on the right one $u_{right} = 0.9$.

on-axis choice (12) with $n = 2$. The continuous curve therein represents a static equilibrium ($M_0^2 = \gamma_1 = 0$) for which current reversal is not possible as already mentioned in section 1. Central current reversal occurs at a critical value of $(\gamma_1)_c = 3.0$, nearly irrespective of the value of the parallel-flow parameter M_0^2 [see Eqs. (3) and (12)]. This result is consistent with that of [30] where purely toroidal flow was considered. To check that the parallel flow has no appreciable impact on the central current reversal we also employed the peaked off-axis flow profile (13) with $m = n = 2$. The results respective to those of Fig. 5 are shown in Fig. 6. Apparently the current density profiles therein are identical with those of Fig. 5 in the close vicinity of the magnetic axis. The off-axis flow, though, makes the region of current reversal narrower.

The pressure of the equilibrium of Fig. 2 monotonically decreases from the magnetic axis to the plasma boundary as can be seen in Fig. 7. In addition, the safety factor monotonically increasing from the magnetic axis to the plasma boundary is shown in Fig. 8.

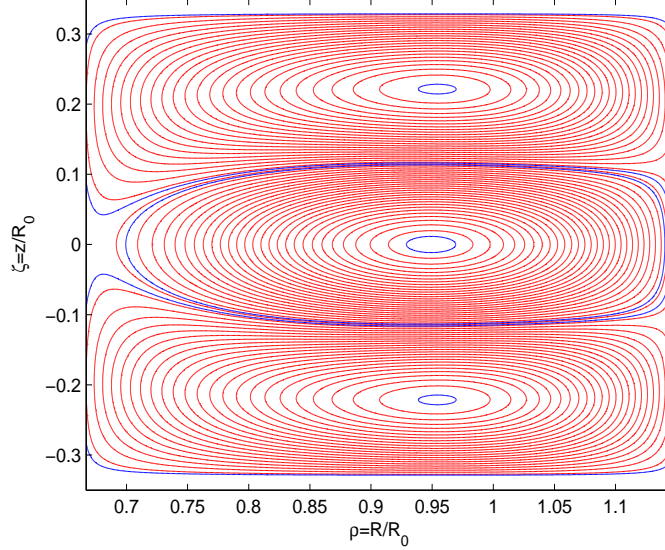


Figure 4: The third equilibrium with non-nested magnetic surfaces described in the text. The boundary of the magnetic lobes, shown in blue, corresponds to the flux value of $u_b = 0$, while at the magnetic axes, as measured from top to bottom we have $u_{a1} = u_{a3} = 0.995$ and $u_{a2} = -1.12$.

Finally, it is noted that current reversal can occur in equilibria with non-nested magnetic surfaces even in the absence of flow [13]-[21].

4 Summary

Solving the GGS equation (6) analytically we have constructed equilibria with incompressible flow, reversed toroidal current density and either nested or non-nested magnetic surfaces. The non-parallel flow results in normal equilibria with nested magnetic surfaces with central current-reversal and monotonically varying pressure profiles. This reversal gets stronger as the non-parallel flow parameter γ_1 in Eq. (11) takes larger values and is nearly unaffected by the parallel component of the flow. Finally, it is noted that the stability of equilibria with non parallel flow remains a tough unsolved problem reflecting the absence of stability criteria even in the framework of hydrodynamics.

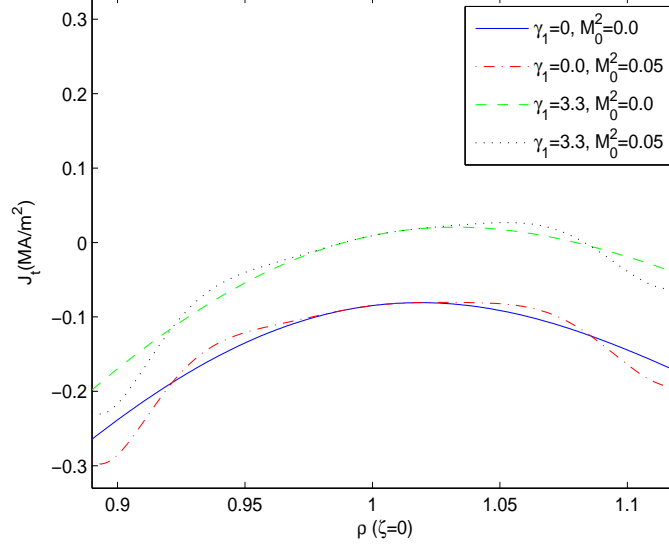


Figure 5: Profiles of the the toroidal current density on the middle-plane $\zeta = 0$ for the equilibrium with nested magnetic surfaces (Fig. 2), for various values of the flow parameters M_0^2 and γ_1 . This refers to the peaked-on-axis choice of Eq. (12). For the green and black curves, we found that on the magnetic axis the value $J_{ta} \simeq 9700 A/m^2 > 0$ and thus indeed current density reversal occurs thereon due to the non-parallel flow (parameter γ_1). The parallel component of the flow associated with M_0^2 hardly affects this reversal.

Acknowledgments

This work has been carried out within the framework of the EUROfusion Consortium and has received funding from the National Programme for the Controlled Thermonuclear Fusion, Hellenic Republic. The views and opinions expressed herein do not necessarily reflect those of the European Commission.

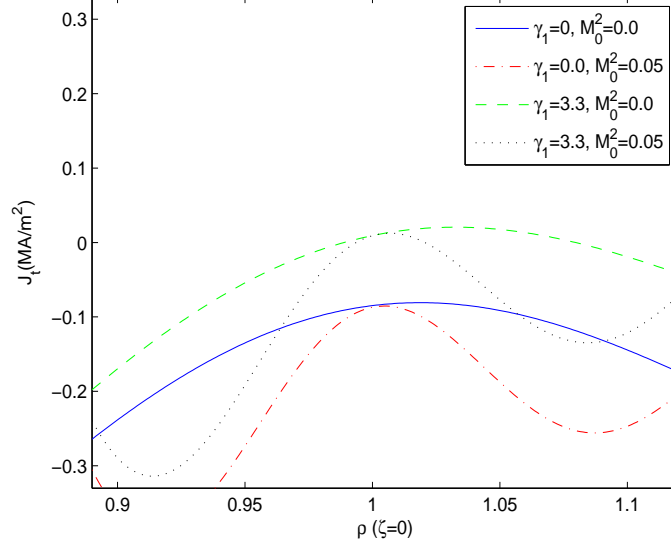


Figure 6: Profiles of the the toroidal current density on the middle-plane $\zeta = 0$ for the equilibrium with nested magnetic surfaces (Fig. 2), for various values of the flow parameters M_0^2 and γ_1 . This refers to the peaked-off-axis choice of Eq. (13).

Appendix: Solution of the homogeneous Eq. (19)

Since Eq. (19), put in canonical form, has a regular singular point at $\rho = 0$ it can be solved by the Frobenius method of infinite convergent series around this point, e.g. [35]. Here we will employ this method slightly modified. Accordingly we try a solution of Eq. (19) of the form

$$U_1 := \sum_{n=0}^{\infty} u_n \rho^n \quad (25)$$

We obtain $u_0 = 0$, u_1 is a freely specified constant which is hereafter, according to standard analysis [35], is set equal to $u_1 = 0.001$, $u_2 = 0$, $u_3 = -\mu^2 u_1 / 8$, $u_4 = 0$ and

$$u_n = -\frac{1}{(n^2 - 1)} [\mu^2 u_{n-2} + \lambda^4 u_{n-4}], \quad (n \geq 5) \quad (26)$$

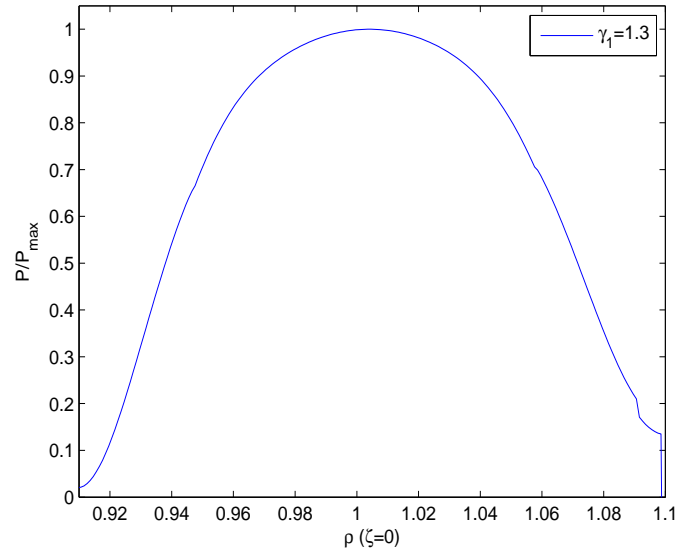


Figure 7: The pressure for the equilibrium of Fig. 2

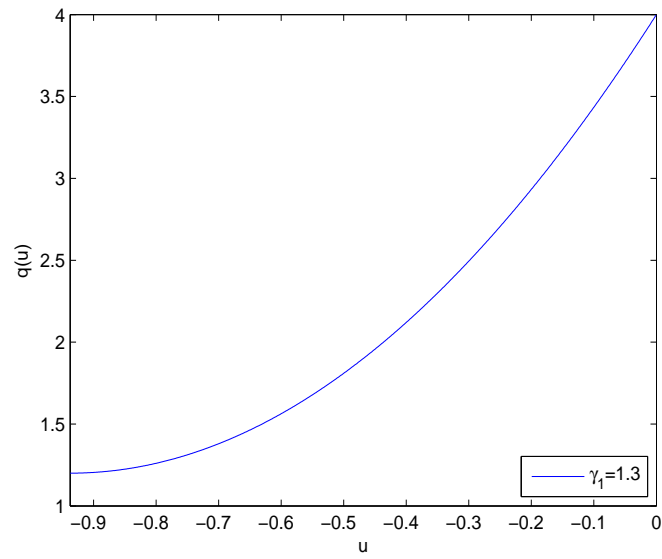


Figure 8: The safety factor for the equilibrium of Fig. 2.

where $\lambda^2 = \mu^2 + \nu^2$. We hereafter call this solution $J_1(\rho; \mu, \nu)$. For sufficiently small values of the parameter μ , J_1 has the usual oscillatory behaviour of the standard Bessel function. More specifically we have found, using extensive numerical tests, that for every $0 < \rho_1 < \rho_2$ there exist numbers ϵ_1, ϵ_2 with $0 < \epsilon_2 < \epsilon_1$ and an integer n_0 such that $|U_1(\rho_1)| < \epsilon_1$ and $|U_1(\rho_2)| < \epsilon_2$ provided that the number of terms n_u used in the series expansion of U_1 satisfies $n_u \geq n_0$. For computational purposes we have retained terms in the series expansion of up to $N_s = 100$.

The second independent solution of Eq. (19) will be of the form

$$U_2 = U_1(\rho) \ln(\rho) + \frac{b_{-1}}{\rho} + \sum_{n=0}^{\infty} b_n \rho^n \quad (27)$$

and obtain $b_0 = 0$, $b_{-1} = -1/\mu^2$. Also, b_1 is a free coefficient which is set, according to the analysis in [35] equal to $b_1 = -0.001$, $b_2 = 0$, $8b_3 = \left(\frac{3\mu^2}{8} + \frac{\lambda^4}{\mu^2} - b_1\mu^2\right)$, $b_4 = 0$ and

$$(n^2 - 1)b_n = -2nb_n - \mu^2 b_{n-2} - \lambda^4 b_{n-4}, \quad (n \geq 5) \quad (28)$$

We call this solution hereafter $Y_1(\rho; \mu, \nu)$.

Since the closest singular point of (19) to $\rho = 0$ is infinity, solutions $J_1(\rho; \mu, \nu)$ and $Y_1(\rho; \mu, \nu)$ converge for any finite value of ρ .

References

- [1] R. C. Wolf, Plasma Phys. Control. Fusion **45**, R1 (2003).
- [2] P. C. de Vries, E. Joffrin et al., Nucl. Fusion **49**, 075007 (2009).
- [3] M. W. Shafer, G. R. McKee, M. E. Austin et al., Phys. Rev. Lett. **103**, 075004 (2009).
- [4] T. Fujita, Nucl. Fusion **87** 245001 (2001).
- [5] N. C. Hawkes, B. C. Stratton et. al., Phys. Rev. Lett. **87**, 115001 (2001).
- [6] T. Fujita, T. Oikawa et. al., Phys. Rev. Lett. **87** 245001 (2001).
- [7] G. T. A. Huysmans, T. C. Hender, N. C. Hawkes, and X. Litaudon, Phys. Rev. Lett. **87**, 245002 (2001).

- [8] M. S. Chu and P. B. Parks, Phys. Plasmas **9**, 5036 (2002).
- [9] G. W. Hammett, S. C. Jardin and B. C. Stratton, Phys. Plasmas **10**, 4048 (2003).
- [10] J. A. Breslau, S. C. Jardin, and W. Park, Phys. Plasmas **10**, 1665 (2003).
- [11] P. Rodrigues and J. P. S. Bizarro, Phys. Plasmas **19**, 012504 (2012).
- [12] J.-J. Aly, Phys. Plasmas **19**, 072517 (2012).
- [13] A. A. Martynov, S. Yu. Medvedev and L. Villard, Phys. Rev. Lett. **91**, 085004 (2003).
- [14] S. Wang, Phys. Rev. Lett. **93**, 155007 (2004).
- [15] S. Wang and J. Yu, Phys. Plasmas **12**, 062501 (2005).
- [16] P. Rodrigues and J. P. S. Bizarro, Phys. Rev. Lett. **95**, 015001 (2005).
- [17] J. Yu, S. Wang, and J. Li, Phys. Plasmas **13**, 054501 (2006).
- [18] P. Rodrigues and J. P. S. Bizarro, J. Plasma Physics **72**, 1209 (2006).
- [19] D. Apostolaki, G. N. Throumoulopoulos, H. Tasso, 35th EPS Conference on Plasma Physics, Crete, 9-13 June 2008, ECA **27**, P2-057 (2008).
- [20] Y. Hu, Phys. Plasmas **15**, 022505 (2008).
- [21] C. G. L. Martins, M. Roberto, I. L. Caldas, and F. L. Braga, Phys. Plasmas **18**, 082508 (2011).
- [22] G.O. Ludwig, P. Rodrigues and J. P.S. Bizarro, Nucl. Fusion **53**, 053001 (2013).
- [23] F. L. Braga, Plasma Science and Technology **15**, 985 (2013).
- [24] Y. Hu, Y. Hu and N. Xiang, Phys. Plasmas **23**, 042506 (2016).
- [25] B. Bartoloni, A. B. Schelin, I.L.Caldas, Phys. Lett. **380A**, 2416 (2016).
- [26] O. Mitarai, A. Hirose, H.M. Skarsgard, Nucl. Fusion **32**, 1801, (1992).
- [27] J. Huang, X. Yang, S. Zheng et al. Nucl. Fusion **40**, 2023, (2000).

- [28] P. Rodrigues and J. P. S. Bizarro, Phys. Rev. Lett. **97**, 125001 (2007).
- [29] J. Li, J. Luo, S. Wang et al., Nucl. Fusion **47**, 1071, (2007).
- [30] Yu. I. Pozdnyakov, Phys. Plasmas **12**, 084503 (2005).
- [31] H. Tasso and G. N. Throumoulopoulos, Phys. Plasmas **5**, 2378 (1998).
- [32] Ch. Simintzis, G. N. Throumoulopoulos, G. Pantis and H. Tasso, Phys. Plasmas **8**, 2641 (2001).
- [33] G. N. Throumoulopoulos, H. Tasso, G. Poulipoulis, J. Plasma Physics **74**, 327 (2008).
- [34] E. K. Maschke, Plasma Phys. **15**, 535 (1973). 052514 (2016).
- [35] C F Chun Man Fong, D De Kee, P N Kaloni, *Advanced Mathematics for Engineering and Science*, World Scientific Publishing Co. Ltd (2003).